JOURNAL OF GUIDANCE, CONTROL, AND DYNAMICS
Vol. 17, No. 6, November–December 1994

Deployment Control of a Cable Connecting a Ship to an Underwater Vehicle

Arun K. Banerjee* and Van N. Do†
Lockheed Missiles & Space Company, Sunnyvale, California 94089

This paper describes the development of an underwater cable dynamics model and a realistic control system that allows deployment, regulation, and retrieval of an unmanned underwater vehicle tethered to a ship. An order-*n* algorithm for a variable-mass cable subject to hydrodynamic forces and motion constraints is used to simulate the dynamics of the system. The dynamics of the underwater vehicle is separately given with the cable tension nonlinearly affecting the vehicle speed. This creates a constraint on the cable motion that depends nonlinearly on the constraint force, a problem that is iteratively solved using constraint stabilization. The cable dynamics model and the controller presented in this paper can be used to answer many design questions relating to tethered underwater vehicles.

I. Introduction

FIGURE 1 shows an unmanned underwater vehicle (UUV) connected to a ship by means of a cable. In this scenario the UUV functions as a guide dog leading the ship through a field of clustered mines attached to the sea floor. The cable can be used to 1) transfer sonar information from the UUV to the ship, 2) transfer guidance and control commands from the ship to the UUV, and 3) transfer power from the ship to the UUV while performing long-range search missions. This paper is concerned with the dynamics and control of such a system.

A critical element in this analysis is the modeling of the cable subjected to hydrodynamic forces and end-motion constraints. Underwater cable dynamics has been studied by many authors (see, e.g., Refs. 1–3). In the present context, the cable is usually treated as a variable-mass system because the motion of the ship, which has a mass several orders of magnitude greater than that of the cable, is assumed to be unaffected by the cable deployment. Reference 1 describes such a variable-length cable by a finite element model consisting of a constant number of beams of variable length and zero flexural rigidity. The present paper builds on these previous works. It retains the variable-element-length feature of Ref. 1 but considers the segments rigid, as in Refs. 2 and 3, allowing large rotation between segments to represent large curvature of the cable. References 2 and 3 use an algorithm that requires decomposing an $n \times n$ mass matrix for the evaluation of the highest derivatives. The arithmetic operation count for this task is of the order n^3. In contrast, the present paper uses a method for which the arithmetic operation count is of order n, as in Refs. 4–6, and because of this, the formulation becomes highly suitable for on-line simulation.

A unique feature of the theory given here is that it is applicable in a situation where an independent analysis of the dynamics of the UUV exists and accounts for its complex hydrodynamic and propulsion forces. The cable tension on the UUV acts as a disturbance on its control system that tries to keep the velocity of the vehicle between some limits. The cable dynamics analysis, which is thus forced to be separate from the UUV analysis, is required to maintain the constraint of connectivity between the cable and the UUV. The nonlinear nature of the tension-velocity relation in the UUV model gives rise to a nonlinear constraint problem where the cable tension depends nonlinearly on the acceleration of the end point of the cable attached to the UUV. A brief outline of the order-n algorithm for constrained systems, along with a resolution of the constraint-control coupling, is given in Sec. II. The cable deployment control law is given in Sec. III. Section IV describes simplified models of UUV and ship dynamics used in the simulation. The results of simulating deployment, stationkeeping, and retrieval of the tethered UUV are presented next. Such results can be used to answer many questions on the design of tethered underwater vehicles.

Received June 17, 1993; revision received May 13, 1994; accepted for publication June 1, 1994.

*Senior Staff Engineer, Lockheed Palo Alto Research Laboratory. Associate Fellow AIAA.

†Research Scientist.

II. Dynamics of Underwater Cable Deployment

Modeling of the dynamics of a cable being reeled out of a moving ship to an underwater maneuvering vehicle requires a method that can describe large curvature of the cable while accounting for the deployment process. In this paper the cable is considered highly flexible but incapable of extension, and torsion is neglected for our purpose. Thus the cable is modeled as a chain of rigid rods connected one to another by two-degree-of-freedom hinges with soft rotational springs that can describe large bending of the cable in two planes. During deployment the cable as a whole undergoes a mass influx in its control volume. Mass transfer in the current curved configuration of the cable is described by increasing the length of all the rods in the chain and including an appropriate boundary force. The dynamics of an n-body system with motion constraints is described for computational efficiency by an order-n algorithm for constrained systems, as in Ref. 7, and is summarized below for convenience.

A. Order-*n* Algorithm for Constrained Systems

Refer to Fig. 2. Let λ be the unknown tension on the cable applied by the UUV. Then considering the free-body diagram of the nth rod and summing inertia and all external forces excluding the force from the $(n-1)$th rod and taking the moment of these forces about the hinge point Q_n, excluding the torque applied by the $(n-1)$th rod, one can write the following, where all vectors have been resolved in the nth body basis:

$$\begin{Bmatrix} f^{*n} - f_e^n - \lambda \\ t^{*n} - t_e^n - \tilde{L}\lambda \end{Bmatrix} = M^n \begin{Bmatrix} a_0^{Q_n} \\ \alpha_0^n \end{Bmatrix} + X^n - H^n\lambda \tag{1}$$

where f^{*n} and f_e^n are the inertia and restricted external force as noted above and t^{*n} and t_e^n are the inertia and restricted external torque on the nth body,

$$M^n = \begin{bmatrix} m^n & -\tilde{S}^n \\ \tilde{S}^n & I^n \end{bmatrix}, \qquad H^n = \begin{bmatrix} U \\ \tilde{L} \end{bmatrix} \tag{2}$$

$$X^n = M^n \begin{Bmatrix} a_t^{Q_n} \\ \alpha_t^n \end{Bmatrix} + \begin{Bmatrix} \tilde{\omega}^n\tilde{\omega}^n S^n - f_e^n \\ \tilde{\omega}^n I^n \omega^n - t_e^n \end{Bmatrix} \tag{3}$$

Here S^n and I^n are the first and second moments of the mass about Q_n, U is the 3×3 identity matrix, and ω^n is the angular velocity

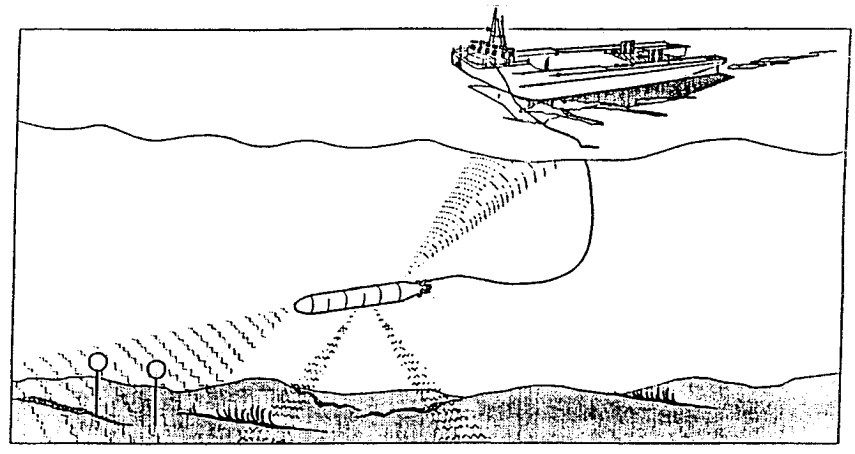

Fig. 1 System configuration.

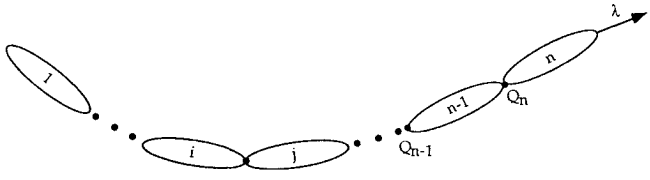

Fig. 2 Discretization of cable.

of body n. Notations with a tilde indicate skew-symmetric matrices formed out of 3×1 matrices for vector cross products; thus $\tilde{L}$ is formed out of a matrix whose first element is L, the length of the rod segment, the other two elements being zero. Symbols in Eq. (1) with zero subscript represent the groups of all terms that involve second derivatives of the generalized coordinates, and those in Eq. (3) with subscript t denote the remainder terms in the acceleration of the hinge point Q_n and the angular acceleration of the body frame n,

$$\begin{Bmatrix} a^{Q_n} \\ \alpha^n \end{Bmatrix} = \begin{Bmatrix} a_0^{Q_n} \\ \alpha_0^n \end{Bmatrix} + \begin{Bmatrix} a_t^{Q_n} \\ \alpha_t^n \end{Bmatrix} \tag{4}$$

Now, exposing the contribution of the two-degree-of-freedom relative rotation at the n hinge, represented by θ^n, one can further write symbolically

$$\begin{Bmatrix} a_0^{Q_n} \\ \alpha_0^n \end{Bmatrix} = \begin{Bmatrix} \hat{a}_0^{Q_n} \\ \hat{\alpha}_0^n \end{Bmatrix} + R^n \ddot{\theta} \tag{5}$$

where the new symbols with the "hat" notation denote the groups of acceleration and angular acceleration terms involving $\ddot{\theta}^1, \ldots, \ddot{\theta}^{n-1}$. The term R^n appearing in Eq. (5) is the 6×2 matrix of the partial velocity of Q_n and the partial angular velocity of body n (see Ref. 8). Substituting Eq. (5) in Eq. (1) and premultiplying the resulting equation by R^{nT}, one gets Kane's equations (Ref. 8) associated with θ^n, in which nonworking constraint forces do not appear:

$$\ddot{\theta}^n = -v_n^{-1} R^{nT} \left[M^n \begin{Bmatrix} \hat{a}_0^{Q_n} \\ \hat{\alpha}_0^n \end{Bmatrix} + X^n - H^n \lambda \right] + v_n^{-1} \tau^n \tag{6}$$

where $v_n = R^{nT} M^n R^n$ and τ^n is the hinge torque applied by body $n-1$ on body n. Use of Eqs. (6) and (5) in Eq. (1) leads to

$$\begin{Bmatrix} f^{*n} - f_e^n - \lambda \\ t^{*n} - t_e^n - \tilde{L}\lambda \end{Bmatrix} = M \begin{Bmatrix} \hat{a}_0^{Q_n} \\ \hat{\alpha}_0^n \end{Bmatrix} + X - H\lambda \tag{7}$$

where the following definitions have been used, with U now a 6×6 identity matrix:

$$\begin{aligned} M &= PM^n, \qquad P = U - M^n R^n v_n^{-1} R^{nT} \\ X &= PX^n \\ H &= PH^n \end{aligned} \tag{8}$$

Now, the kinematics relating the motion of inboard body $n-1$ to that of body n suggests the definition of a shift transform W^n:

$$\begin{Bmatrix} \hat{a}_0^{Q_n} \\ \hat{\alpha}_0^n \end{Bmatrix} = W^n \begin{Bmatrix} a_0^{Q_{n-1}} \\ \alpha_0^{n-1} \end{Bmatrix},$$

$$W^n = \begin{bmatrix} C_{n,n-1} & -C_{n,n-1}\tilde{L} \\ 0 & C_{n,n-1} \end{bmatrix} \tag{9}$$

Here $C_{n,n-1}$ is the coordinate transformation relating the nth body vector basis to the $(n-1)$th body basis. The same shift transform serves to convert the forces and moments from the hinge Q_n to a statically equivalent system at the hinge Q_{n-1}, resulting in

$$\begin{Bmatrix} f^{*n} - f_e^n - \lambda \\ t^{*n} - t_e^n - \tilde{L}\lambda \end{Bmatrix} = W^{nT} \left(MW^n \begin{Bmatrix} a_0^{Q_{n-1}} \\ \alpha_0^{n-1} \end{Bmatrix} + X - H\lambda \right) \tag{10}$$

Now considering the free-body diagram of the $(n-1)$th body, adding the inertia and all external forces including hinge forces from body $n-2$ to body $n-1$ with the force system represented by Eq. (10), and recalling that nonworking constraint forces are eliminated, one gets

$$\begin{Bmatrix} f^{*n-1} - f_e^{n-1} \\ t^{*n-1} - t_e^{n-1} \end{Bmatrix} = M^{n-1} \begin{Bmatrix} a_0^{Q_{n-1}} \\ \alpha_0^{n-1} \end{Bmatrix} + X^{n-1} - H^{n-1}\lambda \tag{11}$$

where one has defined the updates

$$\begin{aligned} M^{n-1} &\leftarrow M^{n-1} + W^{nT} M W^n \\ X^{n-1} &\leftarrow X^{n-1} + W^{nT} X \\ H^{n-1} &= W^{nT} H \end{aligned} \tag{12}$$

Equation (11) is just like Eq. (1). This completes a cycle that is repeated by going backward, considering body $n-2$, $n-3$, etc., in succession, until one encounters body 1, for which the inboard motion (ship motion in this case) is known. The equations for the hinge degrees of freedom for the first link connected to the ship, in this case, can be written as

$$\ddot{\theta}^1 = f_1^1 + c_1^1 \lambda \tag{13}$$

where

$$f_1^1 = -v_1^{-1} R^{1T} X^1 + v_1^{-1} \tau^1, \qquad c_1^1 = v_1^{-1} R^{1T} H^1 \tag{14}$$

For body 1, Eq. (5) yields

$$\begin{Bmatrix} a_0^{Q_1} \\ \alpha_0^1 \end{Bmatrix} = g^1 + h^1 \lambda \tag{15}$$

where

$$g^1 = R^1 f_1^1, \qquad h^1 = R^1 c_1^1 \tag{16}$$

Equation (9) now becomes, for a generic jth body,

$$\begin{Bmatrix} \hat{a}_0^{Q_j} \\ \hat{\alpha}_0^j \end{Bmatrix} = e^j + n^j\lambda \tag{17}$$

where the kinematic shift operation from body i, the inboard body of j to body j, produced

$$e^j = W^j g^i, \qquad n^j = W^j h^i \tag{18}$$

This defines the generic hinge rotation equations

$$\ddot{\theta}^j = f_1^j + c_1^j\lambda \tag{19}$$

where

$$f_1^j = -v_j^{-1}R^{jT}(M^j e^j + X^j),$$

$$c_1^j = -v_j^{-1}R^{jT}(M^j n^j - H^j) \tag{20}$$

Use of Eqs. (19) and (17) in Eq. (5) and the definitions

$$g^j = e^j + R^j f_1^j, \qquad h^j = n^j + R^j c_1^j \tag{21}$$

provide the general relation

$$\begin{Bmatrix} a_0^{Q_j} \\ \alpha_0^j \end{Bmatrix} = g^j + h^j\lambda \tag{22}$$

The stage is now set for uncovering all the dynamic equations in a so-called forward path, going from body 2 to body n.

B. External Forces on Cable

For steady flow, the force exerted by a fluid on a submerged accelerating body is composed of two components, one depending on fluid friction and the other on displaced fluid inertia.[8,10] The transverse oscillatory force on the cable due to vortex shedding is being ignored here for a simple, planar simulation. For cylindrical bodies, the force due to viscous drag is given by

$$\bar{f}_d = -0.5\rho_w\left[\pi DLC_f|v_1|v_1\bar{b}_1 + DlC_{dn}\right.$$

$$\left.\times(v_2\bar{b}_2 + v_3\bar{b}_3)\sqrt{v_2^2 + v_3^2}\right] \tag{23}$$

Here ρ_w is the density of sea water, D is the cable diameter, L is the cable length, C_f is the axial friction coefficient, C_{dn} is the drag coefficient, and v_1, v_2, and v_3 are the body components of the velocity of the body relative to the water, taking into account water current effects. The force required to move the displaced fluid is treated as an added mass effect in the inertia force computation. The apparent mass lumped at the mass center of a rigid link is given as in Ref. 10:

$$m' = L\left(m + C_m\rho_w\pi D^2/4\right) \tag{24}$$

where m is the mass per unit length of the cable, L is the segment length, and C_m is the fluid mass coefficient. Note that Eq. (24), although simplifying matters, does not rigorously treat the physics of fluid inertia in the sense that only acceleration components perpendicular to the cable will affect the apparent fluid mass. In addition to these effects, the force of buoyancy reduces the force of gravity on the rod segments, giving rise to a force of "wet weight" approximately given by

$$\bar{f}_w = -\pi DL(\rho_c - \rho_w)g\bar{n}_2 \tag{25}$$

where ρ_c is the cable density and g is the acceleration due to gravity acting along the vector $\bar{n}_2$.

Finally, we consider the force at the end of the cable due to mass gain (loss) associated with our treatment of deployment (retrieval). This force, as traditionally used in the nature of a thrust, can be represented as a force acting on the link closest to the ship as follows:

$$\bar{f}_t^1 = -(\pi/4)D^2\rho_c\dot{L}\left[\left(v_1^1 - \dot{L}\right)\bar{b}_1^1 + v_2^1\bar{b}_2^1 + v_3^1\bar{b}_3^1\right] \tag{26}$$

where $\dot{L}$ is the deployment rate and v_1^1 and $\bar{b}_1^1$ are, respectively, the axial component of the velocity vector and the unit vector along the axis for body 1, etc.

C. Constraint Stabilization, Control-Constraint Coupling, and Constraint Force

With one end of the cable attached to the ship, the other end is made to move with the UUV, which has its own model and embedded propulsion control system. This implies the existence of a holonomic constraint, which means some of the generalized coordinates are dependent (noted by subscript d in the following) on the independent ones (denoted with subscript i). This in turn means Eqs. (19) can be written in matrix form as

$$\ddot{\theta}_i = F_i + C_i\lambda \tag{27}$$

$$\ddot{\theta}_d = F_d + C_d\lambda \tag{28}$$

The constraint force components in λ can be determined by solving Eqs. (27) and (28) simultaneously with the constraint equations. Now, the constraint equation can be stated in terms of an error in the position vectors from the inertial origin to the UUV measured in two ways: (1) once to the ship and then along the cable and (2) to the UUV directly:

$$\bar{e} = \left(\bar{p}^S + \sum_{i=1}^{n} L\bar{b}_1^i\right) - \bar{p}^{\mathrm{UUV}} = 0 \tag{29}$$

where $\bar{p}^S$, $\bar{p}^{\mathrm{UUV}}$ are the position vectors from the inertial origin of the ship and the UUV.

Equation (29) is nonlinear in the angles θ_i, θ_d. Although a differential-algebraic solver can be used to satisfy Eqs. (27–29), this tends to be computationally expensive, defeating the reason for adopting the order-n formulation. One alternative is to differentiate Eq. (29) twice and solve the resulting equation together with Eqs. (27) and (28). However, this gives rise to the well-known problem of constraint violation with time that requires constraint stabilization (Ref. 11). In this paper the following form of the constraint stabilization was found necessary:

$$\ddot{\bar{e}} + k_1\dot{\bar{e}} + k_2\bar{e} + k_3\int_0^t \bar{e}\,d\tau = 0 \tag{30}$$

Equation (30) requires the computation of the velocity and acceleration of the point P of the cable that is attached to the UUV and comparing these, respectively, with the velocity and acceleration of the UUV. Writing the acceleration of P in matrix form as

$$a^P = J_i\ddot{\theta}_i + J_d\ddot{\theta}_d + a_t^P \tag{31}$$

where all vectors have been resolved in the inertial frame, and substituting Eqs. (27) and (28) in Eq. (31), one obtains, from Eq. (30), the following equations determining the cable tension λ:

$$[J_iC_i + J_dC_d]\lambda = a^{\mathrm{UUV}} - \left\{J_iF_i + J_dF_d + a_t^P\right.$$

$$\left. + k_1(v^P - v^{\mathrm{UUV}}) + k_2e + k_3\int_0^t e\,d\tau\right\} \tag{32}$$

where v^P and v^{UUV} are the velocities of the cable end points P and the UUV, respectively. The acceleration of the UUV, a^{UUV} in Eq. (32), is given as an output of the control system for depth and speed control of the UUV. This control system treats the force applied by the cable, λ, as a disturbance, and thus the output acceleration becomes a function of λ. Because of the nonlinearities of the signal limiters used in the implementation of the control laws described in Sec. III, the functional dependence $a^{\mathrm{UUV}}(\lambda)$ of the output acceleration on λ is nonlinear. Thus Eqs. (30) are nonlinear equations in λ, which are iteratively solved for as follows:

$$[J_iC_i + J_dC_d]\lambda^{n+1} = a^{\mathrm{UUV}}(\lambda^n) - \left[J_iF_i + J_dF_d + a_t^P\right.$$

$$\left. + k_1(v^P - v^{\mathrm{UUV}}) + k_2e + k_3\int_0^t e\,d\tau\right] \tag{33}$$

for iteration count $n = 0, 1, 2, \ldots$. The iteration is started with the numerical value of the output acceleration a^{UUV} obtained from the UUV speed and depth controller by neglecting the effect of the (unknown) disturbance force λ. A suitable convergence criterion is used to stop the iterations. Once Eq. (33) is solved for λ, the dynamic equations are known explicitly from Eqs. (27) and (28).

III. Controller Design

Elements of the cable control system studied in this paper include (1) a tension sensor at the UUV end and (2) a cable winch motor (actuator) controlling cable deployment at the ship. It is often desirable to have the ship speed set manually, i.e., to have the control of the ship as free from the cable regulation problem as possible. In this case, the UUV speed should be automatically controlled to maintain a desired offset distance of the two vehicles over long-duration missions. The commanded goal states for the controller are discussed next.

A. Goal State Determination

Multiple objectives must be met by the cable controller. First, cable tension must be kept below some maximum acceptable level. This maximum allowable tension is mainly determined by the cable-breaking tension and the pull capability of the UUV propulsion system. High cable tension reduces cable life expectancy and causes excessive power usage. The latter would result in shortening mine mapping duration. To mitigate these problems, cable tension should be kept low. On the other hand, the cable tension must be bounded on the lower side. Otherwise, excessive cable sagging will occur. Excessive cable sagging can cause the cable to get tangled with seabed rocks, weeds, and other debris. This kind of situation can only be avoided by maintaining the cable tension above some minimum. The required minimum cable tension for an acceptable level of sag depends mainly on cable scope (the arc length of the submerged cable). Larger tension is required with larger cable scope.

Another objective of the cable controller is to maintain the safety of the personnel onboard the host vessel by maintaining a safe distance between the host vessel and the UUV. This offset distance must be above the maximum mine lethal radius. Thus, the maximum mine lethal radius is a factor determining the lower bound of the allowable scope range. The other factor influencing this lower scope bound is the cable-upsetting torque on the UUV. Too short of a cable scope can cause sizable lateral cable tension at the UUV end. This lateral-force component causes a pitch torque on the UUV that it must counteract with a steady fin deflection angle. As a result, too short a scope can degrade UUV maneuverability. Since fin effectiveness depends heavily on UUV speed, the minimum allowable scope is mainly determined by the mine search system operating speed and the UUV depth. Likewise, cable scope cannot be arbitrarily large. The larger the scope, the higher is the cable tension required to counteract cable weight and drag. The presence of these forces put an upper limit on the allowable scope range.

The first step in designing a cable control law is to determine the two desired cable goal states, of scope and tension at the UUV end, that meet the design requirements. These goal states are determined from a separate, steady-state, hydrodynamic analysis for a discrete set of operating points (characterized by system steady speed, UUV depth, and possibly host-vehicle lateral offset). Goal states at other operating points are obtained from this set through linear interpolation.

B. Cable Control Law

Cable deployment, regulation, and retrieval can all be accomplished by one simple but effective control law. Figure 3 shows an overall block diagram of the controller. As seen, the controller consists of two loops. The first loop controls cable tension at the UUV end by controlling winch pay-out rate. Here a proportional-plus-integral (PI) controller is used where the integral part of the controller is implemented with a limited integration with an upper limit of L_S and a lower limit of $-L_S$. The second loop controls cable scope by controlling the speed of the underwater vehicle. Headings of both vehicles are manually controlled by operating personnel onboard the ship. The whole system consists of three gains and three limiters. Simulation shows that stability of the system is maintained

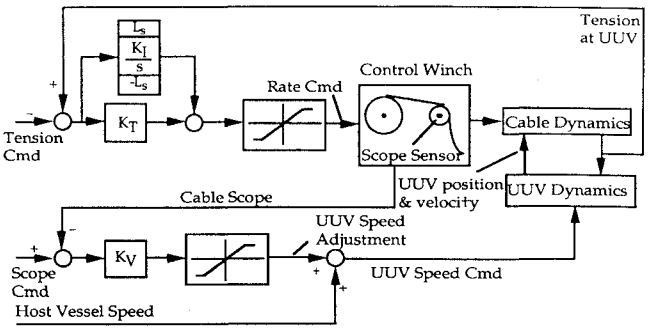

Fig. 3 Cable management law block diagram.

over a wide range of gains. The values of these gains and limiters can be intuitively determined from the desired maximum pay-out/reel-in rate and the ship/UUV maximum speed as follows.

For the mine search system examined, the UUV under a cable tension of 70 lb has the maximum speed of 7.5 ft/s. As a result, if the system is operating at a speed of 6 ft/s, the limiter in the scope loop should be set to 1.5 ft/s to prevent the UUV commanded speed from exceeding the maximum achievable speed. The value of K_V can take on a wide range without affecting system stability. This robustness in stability can be seen as follows. Since the scope rate is approximately the speed difference between the UUV and the ship, we have, for small scope error, it is given by

$$\dot{L} \approx K_V(L_C - L) \tag{34}$$

where L is the cable scope and L_C is the commanded scope. This is a first-order system that is stable at all values of K_V and has a time constant of $1/K_V$. For the application under study, K_V is set to 0.01 so that small scope errors (<150 ft) would be corrected in 5 min (or 300 s). For scope error exceeding 150 ft, the effect of the limiter is felt. Therefore, the time required to correct a large scope error is mainly determined by the limiter in the scope loop.

It is desirable to maintain good cable tension at all time. Hence the bandwidth of the tension loop should be higher than that of the scope loop. For the problem under consideration, the gains in the tension loop are set as follows: 1) $K_T = 0.1$ so that a tension error of 10 lb would cause a scope rate of 1 ft/s; 2) K_I and the integral limiter L_S are set to some small numbers (0.005 and 1 ft/s, respectively) to avoid excessive overshoot; and 3) the tension loop limiter is set to 2.5 ft/s, which is the maximum winch motor rate.

IV. Dynamic Models for the Ship, UUV, and Winch Motor

Because of the relative massive size of the ship, its dynamics is considered unaffected by the cable tension and the overall relation between the commanded ship speed, and the actual position of the ship is well represented by the block diagram of Fig. 4. It is assumed in the cable dynamics analysis that one end of the cable is always attached to the ship. Dynamics of the UUV, as mentioned in Sec. I, is independently given by a separate model that accounts for the complex hydrodynamic and propulsive forces on it. For the purpose of validating the cable control law, simple models of the UUV dynamics is sufficient (see Fig. 5). This vehicle dynamics model includes a speed channel and a depth channel, both affected by cable tension. In Fig. 5, f_v is the vertical tension component and f_s is the cable tension component along the UUV velocity vector. The cable tension acting on the UUV is the vector sum of these two components. The antireset windup (see Ref. 12) used in the integrators in Fig. 5 make the velocity outputs of the UUV nonlinearly dependent on the cable tension, which is seen as a disturbance to the system. As mentioned before, this makes the UUV acceleration a nonlinear function of the cable tension and gives rise to the nonlinear constraint problem. Figure 6 gives a block-diagram representation of the actuator model that is that of a cable winch motor. The motor is modeled with acceleration- and velocity-limited capabilities. Parameters of the simplified ship and UUV models (Figs. 4 and 5) were selected to achieve similar input/output behavior with their corresponding detailed models, with the complex model having gasdynamics and

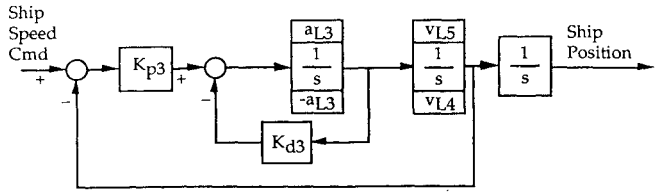

Fig. 4 Simplified host vessel dynamics model.

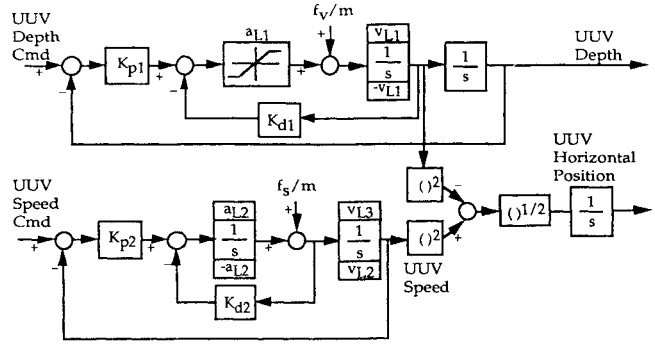

Fig. 5 Simplified UUV dynamics model.

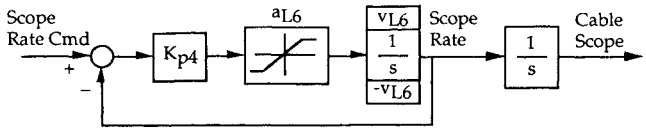

Fig. 6 Simplified cable winch dynamics model.

hydrodynamics taken into consideration over the operational range of interest. The simple winch motor model in Fig. 6 also has excellent input/output matching.

V. Simulation

A computer program incorporating the order-n algorithm for constrained motions and the control system described in this paper was used to simulate deployment, station-keeping, and retrieval of an underwater vehicle tethered to a ship. Equivalent FORTRAN codes describing the block diagrams in Figs. 4–6 were used to complement the cable dynamics. Simulation results are discussed separately below.

Figures 7a–7d show the numerical results for deployment of the cable from an initial length of 1600 ft to a final length of 2200 ft with a commanded tension of 70 lb, with Figs. 7a–7c showing, respectively, the time history of cable length deployed, the tension at the UUV end, and the norm of the constraint error described in Eq. (29). Figure 7d shows snapshots of the shapes of the cable at various instants, where it is to be noted that the scales for the abscissa and the ordinate are made different for clarity. To understand how the system works for deployment, we need to examine the cable control law depicted in Fig. 3. A positive scope error is created when a commanded scope of 2200 ft is entered into the controller. This scope error increases the UUV speed, which in turn causes the two vehicles to move apart. The increase in standoff between the two vehicles causes a higher tension at the UUV. The tension control loop then compensates for this tension increase by paying out more cable. An equilibrium of the system is reached only when both cable tension and scope equal their respective commands.

Figures 8a–8c show the cable length, tension, and constraint error norm for stationkeeping at 1600 ft with the operating tension commanded to be at 70 lb. An initial system transient behavior exists in this simulation because the cable is not initialized at its steady-state hydrodynamic environment. A transient response in the cable dynamics causes reactions from both the scope and tension loops. Again, the system steadies out at the commanded scope and tension.

Figures 9a and 9b show cable length and tension during retrieval of the UUV from 1600 ft to a final cable length of 1000 ft. The behavior of the system in this case is exactly the reverse of the deployment case. Here a negative scope error causes a speed reduction

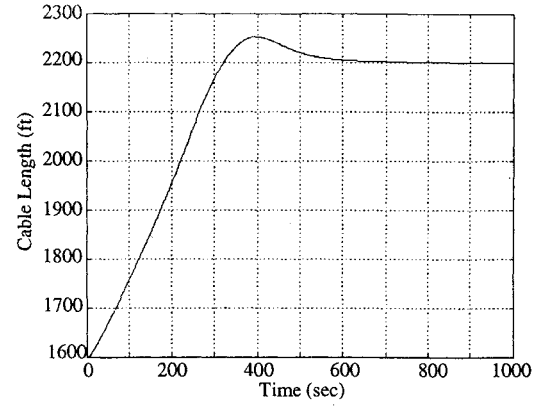

Fig. 7a Cable length vs time during deployment.

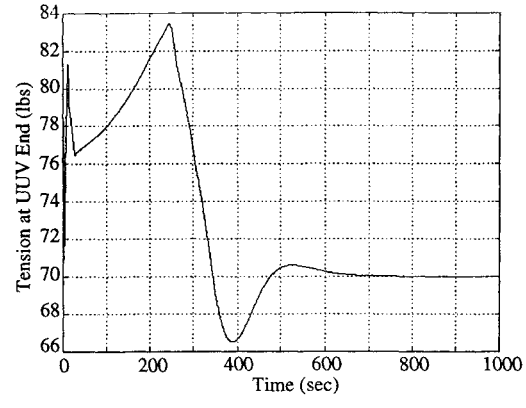

Fig. 7b Cable tension vs time during deployment.

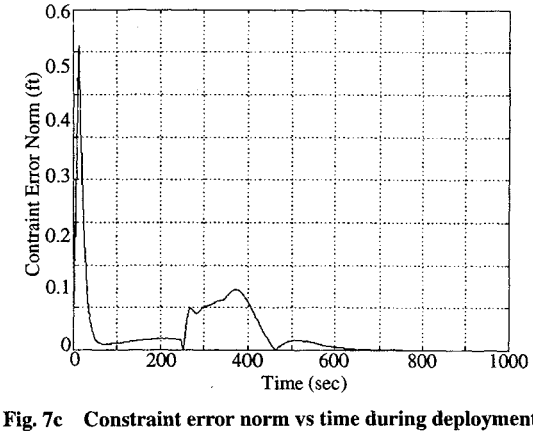

Fig. 7c Constraint error norm vs time during deployment.

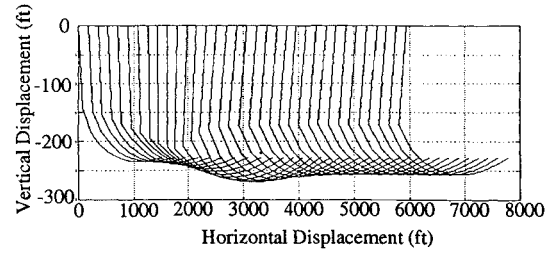

Fig. 7d Cable shapes during deployment.

of the UUV, which in turn produces a drop in cable tension. The tension control loop compensates for this drop in tension by reeling in cable. The system reaches its steady state when both the tension and scope commands are met.

It is seen that in all cases the controller performs satisfactorily. It may be added that, even though the results presented here are for planar maneuvers, the order-n algorithm has been tested for three-dimensional dynamics and works successfully requiring, however, a longer computation time than that for the planar case.

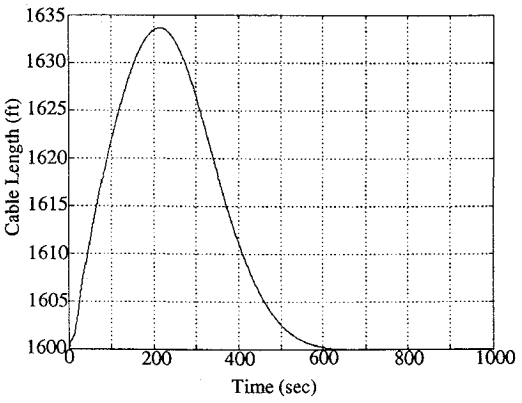

Fig. 8a Cable length vs time during station keeping.

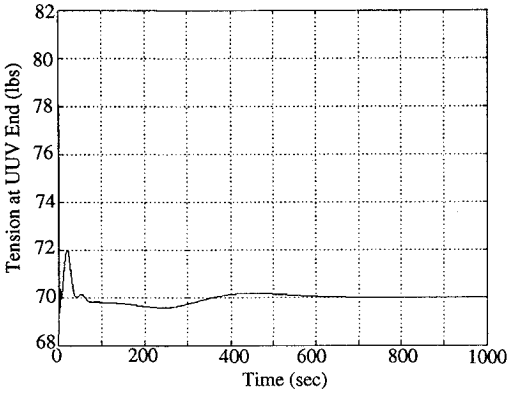

Fig. 8b Cable tension vs time during station keeping.

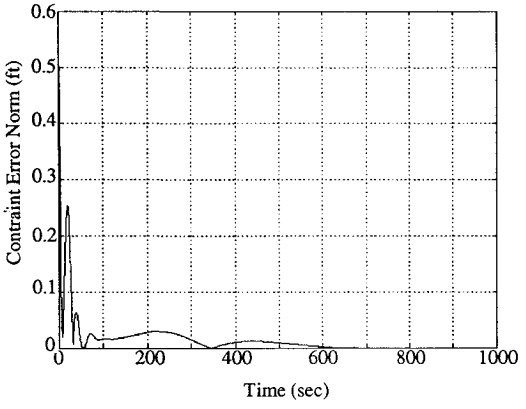

Fig. 8c Constraint error norm vs time during station keeping.

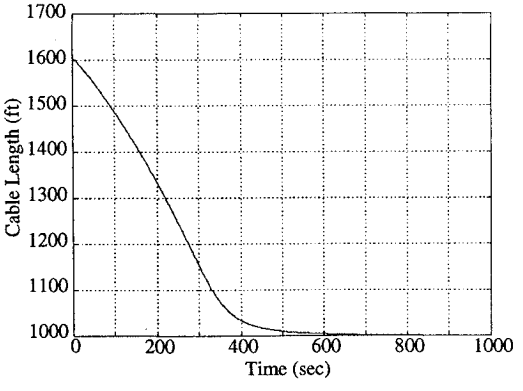

Fig. 9a Cable length vs time during retrieval.

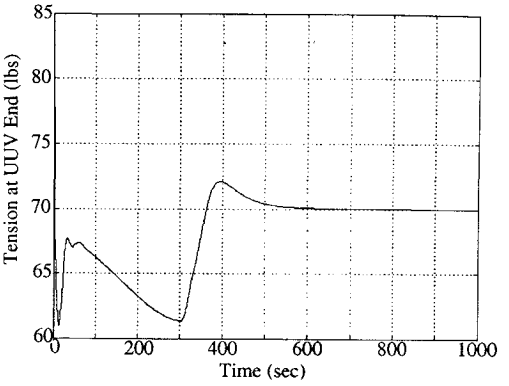

Fig. 9b Cable tension vs time during retrieval.

VI. Summary

The development of an underwater cable dynamics model and a simple but effective cable deployment control law for deployment/regulation/retrieval of an underwater vehicle has been reported in this paper. The dynamics model is suitable for describing large curvature of the cable, and the order-n algorithm given for constrained systems is computationally efficient. A solution procedure is given for the unique problem of nonlinear constraint-control coupling that arises because the dynamics of the underwater vehicle connected to the cable is separately provided. The cable control system design has the desirable properties of simplicity, robustness, and ease of implementation that facilitates transition in operation from cable deployment to cable regulation and finally to cable retrieval. The cable dynamics algorithm and the controller given here can be used to answer many design questions related to the operation of tethered underwater vehicles and robotic devices.

Acknowledgments

The authors are indebted to R. S. Johnstone of Lockheed Advanced Marine System Group for providing them with data for the cable goal states and for his support and guidance in general. They also thank the reviewers for suggesting some clarifications that have been incorporated in the paper.

References

[1]Webster, R. L., "SEADYN Mathematical Manual," Naval Civil Engineering Laboratory, CR-82.019 Port Hueneme, April 1982.

[2]Kamman, J. W., and Huston, R. L., "Modeling of Submerged Cable Dynamics," *Computers and Structures*, Vol. 20, Nos. 1–3, 1985, pp. 623–629.

[3]Khan, N. U., and Ansari, K. A., "On the Dynamics of a Multicomponent Mooring Line," *Computers and Structures*, Vol. 22, No. 3, 1986, pp. 311–334.

[4]Rosenthal, D. E., "An Order-N Formulation for Robotic Systems," *Journal of Astronautical Sciences*, Vol. 38, No. 4, 1990, pp. 511–530.

[5]Banerjee, A. K., "Order-n Formulation of Extrusion of a Beam with Large Bending and Rotation," *Journal of Guidance, Control, and Dynamics*, Vol. 15, No. 1, 1992, pp. 121–127.

[6]Bae, D. S., and Haug, E. J., "A Recursive Formulation for Constrained Mechanical Systems Dynamics: Part II, Closed Loop Systems," *Mechanics of Structures and Machines*, Vol. 15, No. 4, 1987-88, pp. 481–506.

[7]Banerjee, A. K., "Block-Diagonal Equations of Multibody Elastodynamics with Geometric Stiffness and Constraints," *Journal of Guidance, Control, and Dynamics*, Vol. 16, No. 6, 1993, pp. 1092–1100.

[8]Kane, T. R., and Levinson, D. A., *Dynamics*, McGraw-Hill, New York, 1985.

[9]Myers, J. J., Holm, C. H., and McAllister, R. F. (eds.), *Handbook of Ocean and Underwater Engineering*, McGraw-Hill, New York, 1969.

[10]Huston, R. L., and Kamman, J. W., "A Representation of Fluid Forces in Finite Segment Cable Models," *Computers and Structures*, Vol. 14, Nos. 3–4, 1981, pp. 281–287.

[11]Baumgarte, J., "Stabilization of Constraint and Integrals of Motion in Dynamical Systems," *Computer Methods in Applied Mechanics and Engineering*, Vol. 1, 1972, pp. 1–16.

[12]Franklin, G., Powell, J. D., and Emami-Naeni, A., *Feedback Control of Dynamic Systems*, Addision-Wesley, Reading, MA, 1991.